



NATO Undersea Research Centre
Centre de Recherche Sous-Marine de l'OTAN



Reprint Series

NURC-PR-2006-015

Cardioid receive array calibration for active systems

Alberto Baldacci, Georgios Haralabus
Marcel van Velzen.

August 2006

Originally published in:

UDT Europe, Underwater Defence Technology Europe, Hamburg,
Germany, 27-29 June 2006

NATO Undersea Research Centre (NURC)

NURC conducts world class maritime research in support of NATO's operational and transformational requirements. Reporting to the Supreme Allied Commander Transformation, the Centre maintains extensive partnering to expand its research output, promote maritime innovation and foster more rapid implementation of research products.

The Scientific Programme of Work (SPOW) is the core of the Centre's activities and is organized into four Research Thrust Areas:

- Expeditionary Mine Countermeasures (MCM) and Port Protection (EMP)
- Reconnaissance, Surveillance and Undersea Networks (RSN)
- Expeditionary Operations Support (EOS)
- Command and Operational Support (COS)

NURC also provides services to other sponsors through the Supplementary Work Program (SWP). These activities are undertaken to accelerate implementation of new military capabilities for NATO and the Nations, to provide assistance to the Nations, and to ensure that the Centre's maritime capabilities are sustained in a fully productive and economic manner. Examples of supplementary work include ship chartering, military experimentation, collaborative work with or services to Nations and industry.

NURC's plans and operations are extensively and regularly reviewed by outside bodies including peer review of the research, independent national expert oversight, review of proposed deliverables by military user authorities, and independent business process certification. The Scientific Committee of National Representatives, membership of which is open to all NATO nations, provides scientific guidance to the Centre and the Supreme Allied Commander Transformation.



Copyright © NATO Undersea Research Centre 2005. NATO member nations have unlimited rights to use, modify, reproduce, release, perform, display or disclose these materials, and to authorize others to do so for government purposes. Any reproductions marked with this legend must also reproduce these markings. All other rights and uses except those permitted by copyright law are reserved by the copyright owner.

NOTE: The NURC Reprint series reprints papers and articles published by NURC authors in the open literature as an effort to widely disseminate NURC products. Users are encouraged to cite the original article where possible.

CARDIOID RECEIVE ARRAY CALIBRATION FOR ACTIVE SYSTEMS

Alberto Baldacci, Georgios Haralabus, Marcel van Velzen

NATO Undersea Research Centre
 Viale S. Bartolomeo 400, 19138, La Spezia, Italy
 phone: +39 0187 527 302, fax: +39 0187 527 330, email: baldacci@nurc.nato.int
 web: www.nurc.nato.int

ABSTRACT

Nowadays active detection improvement relies significantly on advanced sensor technology, such as the cardioid receive array that allows the directional (right/left) discrimination of the received signal. However, in cardioid sonar signal processing calibration is a major drawback as the signal level obtained is not directly related to the hydrophone pressure level in the water. In this paper, mathematical expressions are derived for the calibration of the cardioid-processed data using CW and LFM signals. The validity of these expressions is demonstrated with simulated and real active LFM sonar data. In addition, two cardioid beamformers are examined and compared; both algorithms are applied to real and modeled data. Comparisons between line and cardioid array are also obtained.

1. INTRODUCTION

Traditional towed line arrays suffer from the well known port/starboard (P/S) ambiguity [1]. This limitation is particularly penalizing, from the sonar performance point of view, in shallow waters, where strong directional reverberation can mask potential targets on both sides of the array [2]. Operational methods have been proposed to overcome this problem, like maneuvering of the towing ship, but these methods are usually time consuming, while single ping P/S discrimination is desirable. Two main categories of arrays capable of discriminating port from starboard have been developed: twin arrays and single line arrays of directional sensors. Cardioid arrays (also called triplet arrays) fall in the latter category. Cardioid arrays are towed arrays consisting of hydrophone triplets. Each triplet is made of three closely-spaced omnidirectional hydrophones evenly mounted on a circle perpendicular to the array axis. By applying proper signal processing, it is possible to make each triplet behave as a single directional hydrophone, by exploiting the small time delay of signals received by the individual hydrophones. Due to the very small distance between sensors, the noise received by the hydrophones of the same triplet is usually strongly correlated and a conventional delay-and-sum beamformer performs poorly. For this reason cardioid beamforming, rather than aiming at the enhancement of the signal coming from the desired steering direction, tries to cancel the signal coming from the ambiguous direction. The drawback of this approach is that cardioid processing returns uncalibrated signal levels.

Calibrated cardioid levels are desirable in some circumstances. As an example, calibrated levels would allow the direct comparison of cardioid beamforming against line array beamforming. Calibrated levels must be known also whenever real data have to be compared with simulated data. In

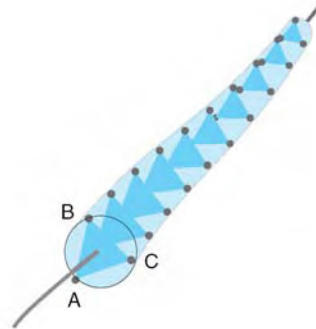


Figure 1: Pictorial representation of a cardioid array (image from [3]).

this paper mathematical expressions are derived for the calibration of the cardioid-processed data using CW signals. The use of such expressions is then extended to frequency-modulated signals (LFM and HFM).

The paper is organized as follows. In section 2 triplet arrays are described more in detail. Cardioid beamforming is illustrated in section 3. The calibration factors for CW and FM signals are derived in section 4. Calibration examples with synthetic and real data are presented in section 5. Finally the conclusions are summarized in section 6.

2. CARDIOID ARRAYS

Cardioid arrays are towed arrays consisting of a line of triplets instead of a line of single hydrophones. Each triplet consists of three closely-spaced omnidirectional hydrophones evenly mounted on a circle perpendicular to the array axis, as shown in figure 1. In this work we adopt a right-handed Cartesian reference system (X, Y, Z) where Y is the array axis pointing at the towing direction, the X axis points at starboard broadside and the Z axis points at the sea surface.

Let K be the number of triplets in the array and let $k = 1, 2, \dots, K$ be the triplet index. Similarly, let $j = 1, 2, 3$ be the index of the hydrophones within each triplet. The angular separation between the sensors in the triplet is denoted with $\gamma = \frac{2}{3}\pi$. Due to the applied forces, the array can be twisted. As a consequence, each triplet will be characterized by a twist angle β_k define clockwise with respect to the Z axis. The angles of each sensor with respect to Z will be denoted with

$$\begin{aligned} \phi_{1k} &= \beta_k \\ \phi_{2k} &= \beta_k + \gamma \\ \phi_{3k} &= \beta_k - \gamma \end{aligned} \quad (1)$$

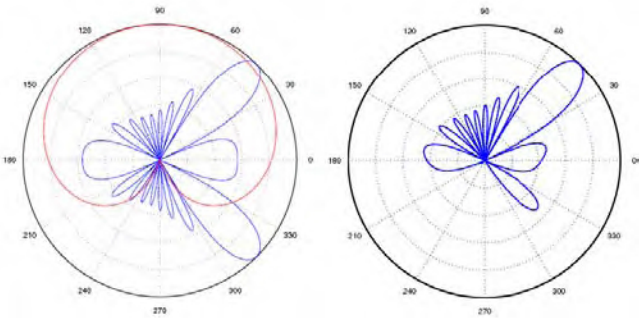


Figure 2: The two steps of cardioid beamforming (image from [3]).

According to this notation, the vector v_{jk} defines the position of the j -th hydrophone within the k -th triplet with respect to the centre of the triplet is

$$v_{jk} = \begin{bmatrix} r \sin \phi_{jk} \\ y_k \\ r \cos \phi_{jk} \end{bmatrix} \quad (2)$$

where r is the radius of the pitch circle the hydrophones are mounted on and y_k is the Y coordinate of the k -th triplet. From the above expression follows that estimation of the array twist is necessary for correct hydrophone positioning. The twist is usually measured by roll sensors evenly distributed along the array.

3. CARDIOID BEAMFORMING

One way of solving the port/starboard ambiguity problem is a special kind of beamforming, called *cardioid beamforming* [3]. The beam pattern obtained from cardioid beamforming corresponds to the beam pattern for a normal line array [4] weighted by the cardioid-shaped beam pattern obtained by combining the data of the three hydrophones in the triplet. This two-step processing is illustrated in fig 2 for a steering direction of 45 degrees. On the left panel, the red line represents the response of the *cardioid hydrophone*, which behaves like a directional hydrophone, and the blue line is the line array beamformer response, characterized by the ambiguous beam at 315 degrees. The final outcome of cardioid beamforming is shown in the right panel, which is the result of the multiplication of the cardioid response by the line array response.

Our implementation of the cardioid beamforming is in the time domain. The cardioid response of each triplet is obtained with the three following steps: (1) the signals received at the triplet sensors are shifted to the triplet centre by applying the proper time delays; (2) the shifted signals are then weighted by the projection of their position vector v_{jk} on the steering direction; (3) the resulting shifted and weighted signals are summed. Since the projection of the v_{jk} vectors on the steering direction can be either positive or negative (depending on the relative positions of the hydrophones with respect of the steering direction), the final result is the difference of the shifted signals, rather than their sum.

We define the steering direction by means of the azimuth angle θ , which runs in the XY plane (i.e. horizontal) clockwise from Y , and of the elevation angle ϕ , which runs in the XZ

plane (i.e. vertical) clockwise from Z . The expression for cardioid beamforming is then

$$b_k(\theta, \phi) = \sum_{j=1}^3 s_{jk}(t - d_{jk}) (u(\theta, \phi) \cdot v_{j,k}) \quad (3)$$

where $u(\theta, \phi)$ is the unit vector defining the steering direction

$$u(\theta, \phi) = \begin{bmatrix} \sin \phi \sin \theta \\ \sin \phi \cos \theta \\ \cos \phi \end{bmatrix} \quad (4)$$

and (\cdot) is the scalar product operator. If we calculate the scalar product we obtain

$$(u(\theta, \phi) \cdot v_{jk}) = r(\sin \phi_{jk} \sin \phi \sin \theta + \cos \phi_{jk} \cos \phi) \quad (5)$$

The above expression is obtained by assuming the centre of the triplet as the origin of a relative reference system, therefore $y_k = 0$.

We now want to calculate the array directivity for a plane wave coming from the steering direction defined by (θ, ϕ) . The signals received at the hydrophones will be related by the following equation

$$s_{jk} = s_k(t + d_{jk}) \quad (6)$$

where

$$d_{jk} = \frac{(u(\theta, \phi) \cdot v_{j,k})}{c} \quad (7)$$

and c is the speed of sound. The array response is then (see Annex 2 for details)

$$b_k(\theta, \phi) = \sum_{j=1}^3 s_k(t) (u(\theta, \phi) \cdot v_{j,k}) = 0 \quad (8)$$

Equation 8 confirms how the cardioid beamforming works: this algorithm places a null in the steering direction. We now have to evaluate the output of the beamformer at the ambiguous direction. Given a plane wave coming from $(-\theta, \phi)$, the signals received at the hydrophones of the k -th triplet are now related by

$$s_{jk} = s_k(t - d_{jk}) \quad (9)$$

The array response to a signal coming from the ambiguous direction b_k^A is therefore (see Annex 2 for details)

$$b_k^A(\theta, \phi) = \sum_{j=1}^3 s_k(t - 2d_{jk}) (u(\theta, \phi) \cdot v_{j,k}) \quad (10)$$

This expression is the output of the single triplet cardioid beamformer and the calibration process consists in finding the relationship between $s(t)$ and $b_k^A(\theta, \phi)$.

4. CALIBRATION

The goal of this section is to derive an analytical relationship between input and output signals of the cardioid beamformer. To this purpose we start considering a continuous wave (CW) signal received at the array. We then extend the results to the case of frequency-modulated (FM) signals.

4.1 Calibration for continuous wave signals

Let us consider a continuous wave signal of amplitude A and frequency f

$$s(t) = A \cos(2\pi ft) \quad (11)$$

By substituting the CW signal in eq. 10 we obtain (see Annex 2 for details)

$$b_k^A(\theta, \phi) = A \cos(2\pi ft) b_1 + A \sin(2\pi ft) b_2 \quad (12)$$

where

$$b_1 = \sum_{j=1}^3 \cos(4\pi f d_{jk}) (u(\theta, \phi) \cdot v_{jk}) \quad (13)$$

and

$$b_2 = \sum_{j=1}^3 \sin(4\pi f d_{jk}) (u(\theta, \phi) \cdot v_{jk}) \quad (14)$$

The explicitation of the above equations for b_1 and b_2 produces expressions which are quite complex. The results presented hereinafter are a simplification of what the general result is, and are chosen to give a better feeling of the behaviour of the coefficient b_1 , b_2 . For sake of simplicity, we can assume that we are interested in horizontal steering directions only, i.e. $\phi = \pi/2$. Under this hypothesis, the scalar product becomes:

$$(u(\theta, \pi/2) \cdot v_{jk}) = r \sin \phi_{jk} \sin \theta \quad (15)$$

By substituting the scalar product in b_1 and b_2 we obtain:

$$b_1 = \sum_{j=1}^3 \cos(4\pi f r / c \sin \phi_{jk} \sin \theta) r \sin \phi_{jk} \sin \theta \quad (16)$$

and

$$b_2 = \sum_{j=1}^3 \sin(4\pi f r / c \sin \phi_{jk} \sin \theta) r \sin \phi_{jk} \sin \theta \quad (17)$$

The above expressions for b_1 and b_2 are still complex and are function of the triplet roll β . Approximated expressions can be obtained if we consider that the argument of the cosinusoidal functions is usually very small. Typical values of the radius r of the array are of the order of $2 \div 2.5$ cm, therefore the argument is of the order of $2 \times 10^{-4} f$. This means that the argument is $\ll 1$ for frequencies of the order of 1KHz, which is a reasonable hypothesis in LFAS applications. As a consequence, the arguments of the cosine and sine functions are $\ll 1$ and we can approximate the cosine and sine functions with their Taylor expansion truncated to the first and third terms, respectively. The resulting approximated expressions are (see Annex 2 for details)

$$\begin{aligned} b_1 &\approx -8(\pi f / c)^2 (r \sin \theta)^3 \sum_{j=1}^3 \sin^3 \phi_{jk} \\ b_2 &\approx 6\pi f (r \sin \theta)^2 / c \end{aligned} \quad (18)$$

Equations 18 suggest two important considerations. The first one is that $|b_1| \ll |b_2|$. In fact it can be demonstrated that the sum is always < 1 . Accordingly, we express b_1 as a function of b_2 as follows:

$$|b_1| \leq -8(\pi f / c)^2 (r \sin \theta)^3 = \frac{4\pi f r}{3c} \sin \theta b_2 \quad (19)$$

where it results that $|b_1| \ll |b_2|$. As a consequence, the output of the cardioid beamformer in the ambiguous direction is still a sinusoidal function, even if in quadrature with respect to the original signal. The relationship between cardioid beamformer input and output signals in case of CW pulses is therefore

$$C_{CW} = 6\pi f (r \sin \theta)^2 / c \quad (20)$$

and the calibration factor is $1/C_{CW}$. The second consideration is that the calibration factor does not depend on the roll factor β_k nor on the steering direction ϕ . These results are confirmed if we plot the exact expressions of b_1 and b_2 for different values of β and f . The coefficient b_1 , plotted in figure 3, shows significant variations with β , especially at higher frequencies. On the other hand, b_2 (plotted in figure 4) is more stable and almost independent on β even at higher frequencies (variations are not visible at this scale). In any case b_1 values are negligible with respect to b_2 values, as can be deduced from the vertical scale of the figures. The ratios between b_1 and the maximum over β of b_2 are approximately 48dB, 34dB, 28dB and 18dB, for frequencies from 100Hz to 3000Hz.

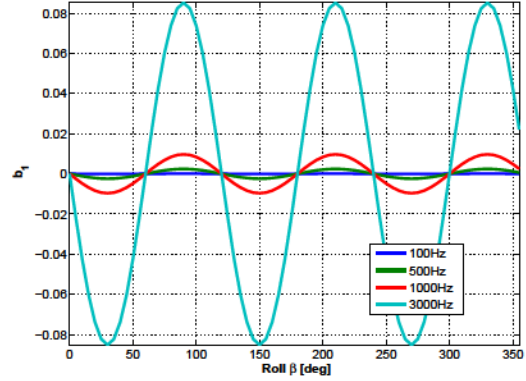


Figure 3: Coefficient b_1 plotted for $\beta = [0;360]$ and $f = [100, 500, 1000, 3000]$ Hz.

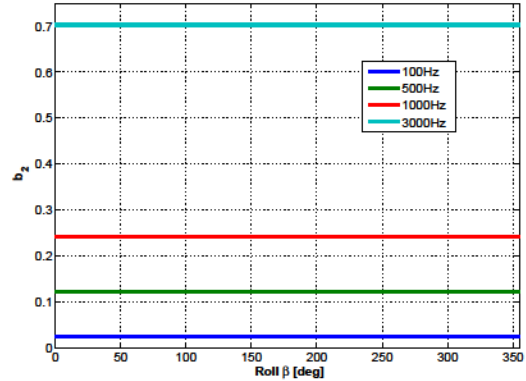


Figure 4: Coefficient b_2 plotted for $\beta = [0;360]$ and $f = [100, 500, 1000, 3000]$ Hz.

4.2 Calibration for frequency modulated signals

In the previous section we derived the calibration factor for the cardioid array in case of CW signals, which results to be

function of the signal frequency, as shown in eq. 20. In case of frequency-modulated (FM) signals, the derivation for CW signals is still approximately valid if the frequency of the signal does not significantly change when we apply the delays d , i.e. if the signals that will be summed still have approximately the same frequency. As the inner triplet hydrophone distance is much smaller than the duration of the incoming wave this is a good approximation. Let us consider, as an example, a linearly frequency-modulated (LFM) signal with centre frequency f_c , bandwidth B and duration T . Its frequency change over the time delay d_{jk} , with respect to the value at time t , is

$$f = f_c - \frac{B}{2} + \frac{B}{2T}(t - d_{jk}) \quad (21)$$

The difference between frequencies for signals received at hydrophones i and j and shifted to the centre of the triplet is

$$\begin{aligned} \Delta f_{ij} &= f_i - f_j \\ &= \frac{B}{2T}(d_j - d_i) \end{aligned} \quad (22)$$

By substituting in eq. 22 the expressions for d of eq. 7 we obtain

$$\Delta f_{ij} = \frac{B}{2T} \frac{r}{c} \sin \theta \sin(\beta \pm \gamma/2) \sin(\pm \gamma/2) \quad (23)$$

This difference has its maxima and minima for $\theta = \pm \pi/2$ and $\beta = \pm \pi/2 \pm \pi/3$, which in absolute level are equal to

$$\Delta f_{MAX} = \frac{B}{2T} \frac{r}{c} \sqrt{3}/2. \quad (24)$$

This maximum frequency difference is acceptable if $\Delta f_{MAX}/f \ll 1$, i.e. if

$$B \ll fT \frac{2c}{r\sqrt{3}} \quad (25)$$

In practical LFAS applications, where the pulse length is of the order of few seconds, this expression is always satisfied and therefore it can be assumed that the calibration factor derived for CW signal also applies to any FM signals. However, the calibration factor is no longer independent of time over the duration of the signal as the frequency itself depends on time. This means that for unknown time of arrival of the signal the beamformer cannot, in principle, be calibrated. Changes relative to the value at the centre frequency by $20 \log(1 \pm B/(2f_c))$ can be significant for a broadband pulse. However, after matched filtering the total signal level will obtain a lower contribution from the part of the signal before the centre frequency but a higher contribution from the part of the signal after the centre frequency and the differences in level will average out. Therefore the FM calibration will be based on the pulse's centre frequency:

$$C_{FM} = 6\pi f_c (r \sin \theta)^2 / c. \quad (26)$$

The validity of this assumption is verified in the next section by means of tests with synthetic and real data.

5. CALIBRATION EXAMPLES

5.1 Synthetic data

Calibrated cardioid beamforming was tested on synthetic data. In this section we present a calibration example based

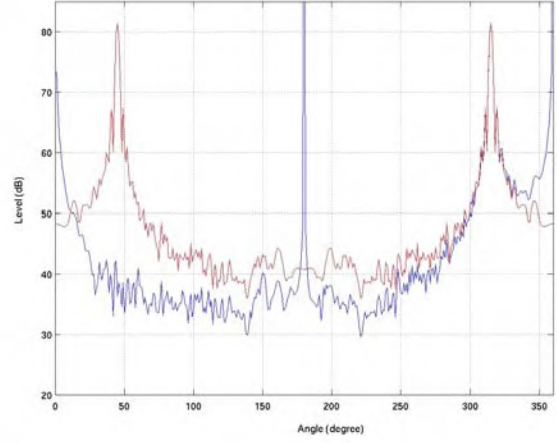


Figure 5: Single line (red) and calibrated cardioid (blue) beam patterns for synthetic data.

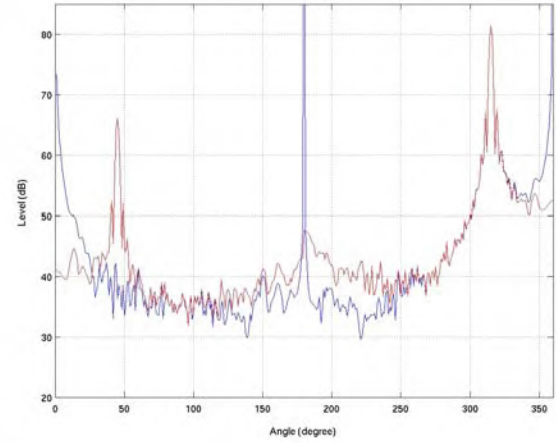


Figure 6: Calibrated standard (blue) and modified (red) beam patterns for synthetic data.

on simulated triplet array data generated for an LFM pulse with centre frequency $f_c = 1200\text{Hz}$, bandwidth $B = 400\text{Hz}$, duration $T = 1\text{s}$ and with a point target at 315 degrees. Synthetic data are cardioid beamformed and calibrated with the calibration factor of eq. 26. Calibrated beamformed data are then matched filtered. The output levels of the matched filter are compared with the levels obtained by line-array beamforming and matched filtering a single line array formed by taking only one hydrophone per triplet. The line array beamformer and the matched filter have 0dB signal gain, meaning that the maximum of the matched filter output corresponds to the maximum amplitude of the signal received at the hydrophones. The noise level is very low in the simulated data and can be neglected. Figure 5 shows the line array response (red line) and the calibrated cardioid array response (blue line) as a function of steering direction. Since the two beam patterns are calibrated, the sidelobe levels can be compared directly. The cardioid beamformer has equal or better sidelobe behavior than the line array beamformer except near endfire where the calibrated cardioid algorithm has a singu-

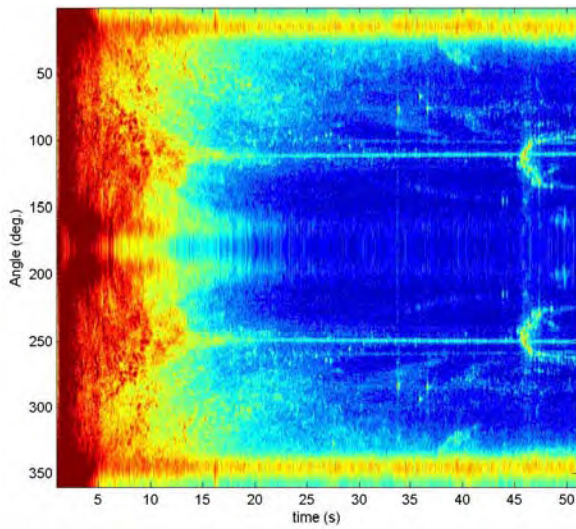


Figure 7: Matched filter output for single-line array beamforming (no target present).

larity, due to the fact that $C_{FM} = 0$ for $\theta = (0, \pi)$, where $\sin \theta = 0$. From a practical point of view, calibrated cardioid processing gives good results up to about 10 degrees from forward or backward endfire. For angles less than 10 degrees from endfire the cardioid beamforming should be replaced by line array beamforming.

In order to avoid the singularity at endfire it is also possible to slightly modify the cardioid algorithm. An alternative implementation places a null at $-\frac{\theta}{|\theta|} \frac{\pi}{2}$, i.e. always at broadside at the ambiguous side. In this case $\sin \theta = \sin(\pm\pi/2) = \pm 1$. The beam patterns obtained with the two cardioid beamforming algorithms are compared in figure 6, where the blue line corresponds to the standard algorithm and the red line corresponds to the modified one. The comparison between the two beam patterns shows that the modified algorithm offers only a 16 dB left-right suppression for a target at 315 degrees, but the singularity at endfire is removed.

5.2 Experimental data

Calibrated cardioid beamforming was tested also with real data collected during the BASE'04 sea trial of the NATO Undersea Research Centre [2]. In this section we show the results obtained for a ping of real active cardioid sonar data corresponding to a LFM pulse with centre frequency $f_c = 1050\text{Hz}$, bandwidth $B = 500\text{Hz}$ and duration $T = 3\text{s}$. No target is present in this example. The line array data is beamformed for 60 beams equally spaced in sine domain and the cardioid array data is beamformed for 120 beams equally spaced in sine domain. Beamformed data are then matched filtered. The calibration results are shown in figure 7-9. The same color scale is used in all images. Figure 7 is the result of line array processing and is symmetric around 180 degrees. Figure 8 shows the results for the standard calibrated cardioid algorithm and the known problems at forward and backward endfire can be observed easily. Figure 9 is the result for the modified cardioid algorithm. For this data set differences in left-right suppression for the standard and modified cardioid algorithms are practically unobservable.

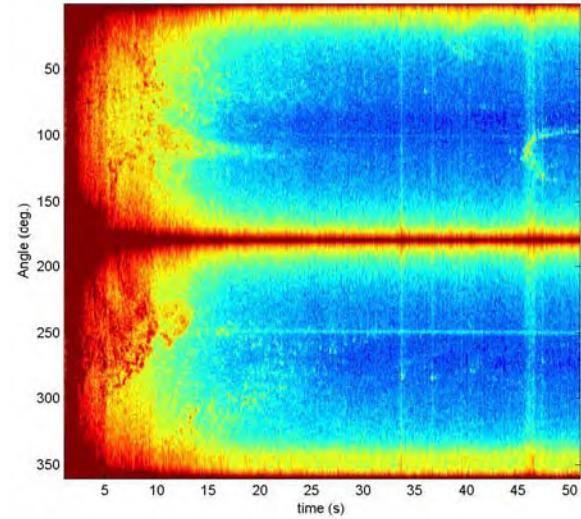


Figure 8: Matched filter output for standard calibrated cardioid beamforming (no target present).

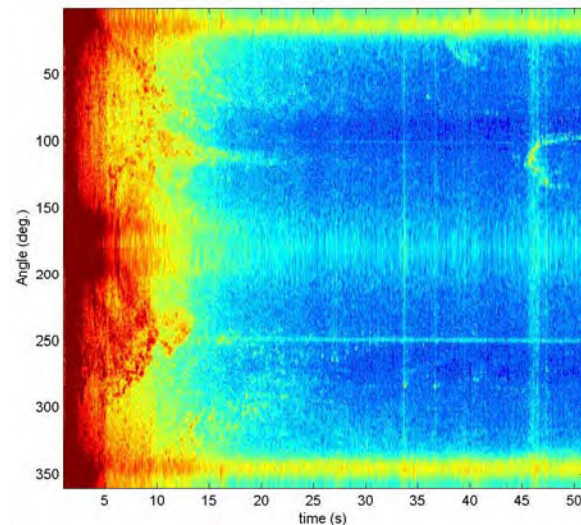


Figure 9: Matched filter output for modified calibrated cardioid beamforming (no target present).

6. CONCLUSIONS

In this paper mathematical expressions for calibration of cardioid array beamforming are derived. The work is based on the analysis of the relationship between signals at the input and output of the cardioid beamformer. The calibration factor for CW signals is shown to be proportional to the frequency of the pulse. Calibration formulae for frequency-modulated signals, such as LFM and HFM, are obtained by extending the results for the CW signals. The cardioid beamformer calibration formulae have been successfully tested with synthetic and real data.

7. ACKNOWLEDGMENTS

The content of this document pertains to work performed under Project 04C3 of the NATO Undersea Research Centre Scientific Programme of Work.

ANNEX 1: USEFUL TRIGONOMETRIC EXPRESSIONS

In the derivation of the cardioid beamformer response we often have to deal with expressions which are sum of three trigonometric functions with arguments ϕ_{jk} . If we substitute to ϕ_{jk} the values of eq. 1, where $\gamma = \frac{2}{3}\pi$, we obtain the following equivalences which are satisfied $\forall \beta$:

$$\begin{aligned} \sin\beta + \sin(\beta + \gamma) + \sin(\beta - \gamma) &= 0 \\ \cos\beta + \cos(\beta + \gamma) + \cos(\beta - \gamma) &= 0 \\ \sin^2(\beta) + \sin^2(\beta + \gamma) + \sin^2(\beta - \gamma) &= 3/2 \\ \cos^2(\beta) + \cos^2(\beta + \gamma) + \cos^2(\beta - \gamma) &= 3/2 \end{aligned} \quad (27)$$

ANNEX 2: DERIVATION OF RESULTS

Derivation of equation 8

$$\begin{aligned} b_k(\theta, \phi) &= \sum_{j=1}^3 s_{jk}(t - d_{jk})(u(\theta, \phi) \cdot v_{j,k}) \\ &= \sum_{j=1}^3 s_k(t + d_{jk} - d_{jk})(u(\theta, \phi) \cdot v_{j,k}) \\ &= \sum_{j=1}^3 s_k(t)(u(\theta, \phi) \cdot v_{j,k}) \\ &= s_k(t)r [\sin\phi \sin\theta \sum_{j=1}^3 \sin\phi_{jk} + \\ &\quad \cos\phi \sum_{j=1}^3 \cos\phi_{jk}] \\ &= 0 \end{aligned} \quad (28)$$

where the last line is obtained by substituting equations 1 in 8 and using the second and third results in Annex 1.

Derivation of equation 10

$$\begin{aligned} b_k^A(\theta, \phi) &= \sum_{j=1}^3 s_{jk}(t - d_{jk})(u(\theta, \phi) \cdot v_{j,k}) \\ &= \sum_{j=1}^3 s_k(t - d_{jk} - d_{jk})(u(\theta, \phi) \cdot v_{j,k}) \\ &= \sum_{j=1}^3 s_k(t - 2d_{jk})(u(\theta, \phi) \cdot v_{j,k}) \end{aligned} \quad (29)$$

Derivation of equation 12

$$\begin{aligned} b_k^A(\theta, \phi) &= \sum_{j=1}^3 A \cos((2\pi f(t - 2d_{jk}))) (u(\theta, \phi) \cdot v_{j,k}) \\ &= A \sum_{j=1}^3 \cos(2\pi ft) \cos(4\pi f d_{jk}) (u(\theta, \phi) \cdot v_{j,k}) + \\ &\quad A \sum_{j=1}^3 \sin(2\pi ft) \sin(4\pi f d_{jk}) (u(\theta, \phi) \cdot v_{j,k}) \\ &= A \cos(2\pi ft) \sum_{j=1}^3 \cos(4\pi f d_{jk}) (u(\theta, \phi) \cdot v_{j,k}) + \\ &\quad A \sin(2\pi ft) \sum_{j=1}^3 \sin(4\pi f d_{jk}) (u(\theta, \phi) \cdot v_{j,k}) \\ &= A \cos(2\pi ft) b_1 + A \sin(2\pi ft) b_2 \end{aligned} \quad (30)$$

Derivation of equation 18

By using the truncated Taylor expansion we can approximate sin and cos with small arguments as:

$$\begin{aligned} \sin\epsilon &\approx \epsilon \\ \cos\epsilon &\approx 1 - \epsilon^2/2 \end{aligned} \quad (31)$$

By substituting the approximations in equations 16,17 we obtain:

$$\begin{aligned} b_1 &\approx \sum_{j=1}^3 (1 - 1/2(4\pi fr/c \sin\phi_{jk} \sin\theta)^2) r \sin\phi_{jk} \sin\theta \\ &= r \sin\theta \sum_{j=1}^3 \sin\phi_{jk} - 8(\pi f/c)^2 (r \sin\theta)^3 \sum_{j=1}^3 \sin^3\phi_{jk} \\ &= -8(\pi f/c)^2 (r \sin\theta)^3 \sum_{j=1}^3 \sin^3\phi_{jk} \end{aligned} \quad (32)$$

and

$$\begin{aligned} b_2 &\approx \sum_{j=1}^3 4\pi fr/c \sin\phi_{jk} \sin\theta r \sin\phi_{jk} \sin\theta \\ &= 4\pi f (r \sin\theta)^2 / c \sum_{j=1}^3 \sin\phi_{jk} \\ &= 6\pi f / c (r \sin\theta)^2 \end{aligned} \quad (33)$$

REFERENCES

- [1] R. J. Urick, *Principles of Underwater Sound*. McGraw-Hill, New York, 1983.
- [2] G. Haralabus, A. Baldacci, R. Laterveer, M. van Velzen, "Broadband active detection in reverberation-limited conditions," in *Proc. of ECUA 2004*, Delft, The Netherlands, July 2004.
- [3] D. T. Hughes, *Aspects of cardioid processing*, SACLANTCEN SR-329, 2000.
- [4] S. Haykin, *Array signal processing*. Prentice-Hall, 1985.

Document Data Sheet

Security Classification RELEASABLE TO THE PUBLIC		Project No.
Document Serial No. NURC-PR-2006-015	Date of Issue August 2006	Total Pages 9 pp.
Author(s) Alberto Baldacci, Georgios Haralabus, Marcel van Velzen		
Title Cardioid receive array calibration for active systems		
Abstract		
Keywords		
Issuing Organization NATO Undersea Research Centre Viale San Bartolomeo 400, 19138 La Spezia, Italy [From N. America: NATO Undersea Research Centre (New York) APO AE 09613-5000]		Tel: +39 0187 527 361 Fax: +39 0187 527 700 E-mail: library@nurc.nato.int